Published in final edited form as:
Neuroscience. 2010 March 17; 166(2): 397–407. doi:10.1016/j.neuroscience.2010.01.005.

Kir4.1 is Responsible for the Native Inward Potassium Conductance of Satellite Glial Cells in Sensory Ganglia

Xiaofang Tang, **Tiffany M. Schmidt**, **Claudio E. Perez-Leighton**, and **Paulo Kofuji**
Department of Neuroscience, University of Minnesota, Minneapolis, MN 55455, USA

Abstract

Satellite glial cells (SGCs) surround primary afferent neurons in sensory ganglia, and increasing evidence has implicated the K^+ channels of SGCs in affecting or regulating sensory ganglion excitability. The inwardly rectifying K^+ (Kir) channel Kir4.1 is highly expressed in several types of glial cells in the central nervous system where it has been implicated in extracellular K^+ concentration buffering. Upon neuronal activity, the extracellular K^+ concentration increases, and if not corrected, causes neuronal depolarization and uncontrolled changes in neuronal excitability. Recently, it has been demonstrated that knockdown of Kir4.1expression in trigeminal ganglia leads to neuronal hyperexcitability in this ganglia and heightened nociception. Thus, we investigated the contribution of Kir4.1 to the membrane K^+ conductance of SGCs in neonatal and adult mouse trigeminal and dorsal root ganglia. Whole cell patch clamp recordings were performed in conjunction with immunocytochemistry and quantitative transcript analysis in various mouse lines. We found that in wild-type mice, the inward K^+ conductance of SGCs is blocked almost completely with extracellular barium, cesium and desipramine, consistent with a conductance mediated by Kir channels. We then utilized mouse lines in which genetic ablation led to partial or complete loss of Kir4.1 expression to assess the role of this channel subunit in SGCs. The inward K^+ currents of SGCs in Kir4.1 +/- mice were decreased by about half while these currents were almost completely absent in Kir4.1 -/- mice. These findings in combination with previous reports support the notion that Kir4.1 is the principal Kir channel type in SGCs. Therefore Kir4.1 emerges as a key regulator of SGC function and possibly neuronal excitability in sensory ganglia.

Keywords

Satellite glial cells; Trigeminal ganglia; Dorsal root ganglia; Kir4.1 channel; KCNJ10; potassium channel; potassium buffering; pain

Primary afferent neurons in sensory ganglia relay various modalities of sensory information from the periphery to the central nervous system. These neurons are tightly enveloped by supporting cells known as satellite glial cells (SGCs) (Hanani, 2005, Ohara et al., 2009). SGCs share many similarities with brain astrocytes including expression of immunocytochemical markers such as the glutamate transporter GLAST, connexin 43, and glutamine synthetase (GS) (Hanani, 2005, Vit et al., 2008). In addition, inwardly rectifying K^+ (Kir) channels are

Address for correspondence: Paulo Kofuji, Department of Neuroscience, University of Minnesota, 6-145 Jackson Hall, 321 Church St SE, Minneapolis, MN 55455, Phone: 612-625-6457, FAX: 612-626-5009, kofuj001@umn.edu.
Section Editor: Cellular Neuroscience, C. Sotelo, Université Pierre et Marie Curie (Paris VI), Paris, France

highly expressed in both astrocytes and SGCs (Gola et al., 1993, Konishi, 1996, Cherkas et al., 2004, Kofuji and Newman, 2004, Dublin and Hanani, 2007). Kir channels are known to exhibit an asymmetrical conductance at hyperpolarized (high conductance) compared to depolarized (low conductance) voltages (Nichols and Lopatin, 1997). Kir channels are also thought to contribute to the deeply hyperpolarized resting membrane potential of glial cells (Butt and Kalsi, 2006, Olsen and Sontheimer, 2008). Moreover, Kir channels are presumed to form the glial K^+ conductive pathways for extracellular K^+ regulation in the nervous system (Konishi, 1996, Kofuji and Newman, 2004). This process, known as spatial K^+ buffering is considered vital for sustaining neuronal activity by limiting changes in extracellular K^+ concentration ($[K^+]_o$) (Kofuji and Newman, 2004).

There is considerable molecular heterogeneity of Kir channels with seven subfamilies of genes (Kir1 to Kir7)(Nichols and Lopatin, 1997, Kubo et al., 2005). Investigation into the molecular composition of Kir channels in CNS glia has demonstrated that Kir4.1 channels (encoded by *KCNJ10* gene) are expressed and constitute the major resting K^+ conductance in astrocytes, retinal Müller cells and oligodendrocytes (Kofuji and Connors, 2003, Butt and Kalsi, 2006, Olsen and Sontheimer, 2008). Channels composed of Kir4.1 have high open probability at resting membrane potentials and only moderate inward rectification (Isomoto et al., 1997). These properties make this subunit ideal to provide the K^+ entry and exit pathways for glial cells as postulated in the spatial K^+ buffering mechanism (Kofuji and Newman, 2004).

It has been reported that immunoreactivity for Kir4.1 is found in trigeminal but not in dorsal root ganglia SGCs (Hibino et al., 1999), suggestive of a differential expression of Kir4.1 among sensory ganglia. Recently, it has been demonstrated that chronic constriction of infraorbital nerve in rats, a common model of orofacial neuropathic pain, leads to downregulation of Kir4.1 expression in trigeminal ganglia SGCs (Vit et al., 2008). Moreover, knockdown of Kir4.1 expression in trigeminal ganglia SGCs using siRNAs induces facial neuropathic pain-like behavior in rats indicating a close relationship between SGC Kir4.1 expression and neuronal excitability (Vit et al., 2008, Ohara et al., 2009).

Despite the potential relevance of Kir4.1 in sensory ganglia, little is known about the relative contribution of this particular subunit in setting the membrane potential and membrane K^+ conductance of SCGs that surround primary sensory neurons. Here we utilized mouse transgenic lines with variable levels of Kir4.1 expression and patch-clamp analysis to evaluate the role of this Kir subunit in SGCs. Our results demonstrate that Kir4.1 constitutes the principal Kir channel subunit expressed in SGCs of trigeminal and dorsal root ganglia and plays a pivotal role in setting the membrane potential and inward K^+ conductance of these cells.

Experimental Procedures

Animals

Generation of Kir4.1 -/- mice and transgenic mice expressing the fluorescent protein EGFP under the Kir4.1 promoter have been described previously (Kofuji et al., 2000, Tang et al., 2009). All animal experiments were performed in accordance with University of Minnesota Institutional Animal Care and Use Committee and National Institutes of Health guidelines.

Antibodies

Primary antibodies used in this study were polyclonal rabbit Kir4.1 (1:1000) (Alomone Labs, Jerusalem, Israel), monoclonal mouse glutamine synthetase (1:500) (Millipore, Billerica, MA), and monoclonal anti neuron specific protein NeuN (1:100)(Millipore). For secondary antibodies, we used AlexaFluor conjugated antibodies (Invitrogen, Carlsbad, CA) produced in goat, including anti-rabbit 568 and anti-mouse 594.

Immunocytochemistry

Adult postnatal day 30 (P30) to P50 mice were sacrificed with CO_2 asphyxiation, and intracardially perfused with 4% paraformaldehyde-0.1 M phosphate buffer solution. Trigeminal and dorsal root ganglia were dissected and post-fixed in the same fixative for 30 min at 4°C. The tissue was then washed in phosphate buffered solution (PBS) and cryoprotected with PBS/30% sucrose for 48 hours, and then cut longitudinally at 10 μm thick slices. In the following day, slices were washed extensively in PBS, and blocked for 1 hr in PBS containing 10% goat serum, 0.5% Triton X-100 at room temperature. Primary antibody incubation was carried out for three days at 4°C in PBS containing 1% goat serum, 0.5% Triton X-100. Sections were then washed 3 × 5 min each in PBS, then incubated in secondary antibodies overnight at 4°C. Sections were again washed 3×5 min in PBS, and then mounted in Vectashield (Vector Laboratories, Burlingame, CA).

Image analysis

The fluorescent specimens were imaged with Olympus Fluoview 1000 confocal microscope (Olympus Inc., Center Valley, PA), using 20×, 40× or 60× oil immersion lens. Optical sections were collected at 0.5- 1.0 μm intervals, and reconstructions of several optical images onto a single plane were performed using Image J software. Scans were further processed into color images using Adobe Photoshop 7.0 (Adobe Systems, San Jose, CA). The brightness and contrast of the images were adjusted using image J software.

Quantitative Reverse Transcriptase Polymerase Chain Reaction (RT-PCR)

RNA samples from dorsal root ganglia and trigeminal ganglia were obtained from adult (P30-P50) and neonatal (P8-P9) wild-type, Kir4.1+/- and Kir4.1-/- mice. Total RNA was extracted using the RNA Easy Kit (Qiagen Inc, Valencia, CA) and RNA was quantified using a NanoDrop-1000 spectrophotometer (Thermo Scientific, Wilmington, DE). Equal amounts of RNA were used for reverse transcription reactions using a Quantitect Reverse Transcription kit (Qiagen Inc.). Real Time PCR reactions for Kir4.1 and β-actin were done in duplicate using the Roche Universal Probe Library System (Roche Applied Sciences, Indianapolis, IN) following manufacturer instructions. For Kir4.1 reactions we employed the following primers: forward primer (5′-agtcttggccctgcctgt-3′), reverse primer (5′-agcgaccgacgtcatctt-3′) and probe #51 from mouse Universal Probe Library (Roche). For β-actin reactions the primers were: forward primer (5′-aaggccaaccgtgaaaagat-3′), reverse primer: 5′-(gtggtacgaccagaggcatac-3′) and probe #56 from mouse Universal Probe Library. Efficiency of the real time PCR reactions was determined in triplicate using the dilution curve method (Pfaffl, 2001). Transcript level of Kir4.1 per sample was calculated as relative to β-actin for each sample using the efficiency corrected ratio (Pfaffl, 2001). Kir4.1 transcript levels were normalized to wild-type expression for both adult and neonatal animals.

Electrophysiology

For adult mice (P30-P50), trigeminal and dorsal root ganglia were removed and stored in ice-cold, oxygenated (95% O_2-5% CO_2) Krebs solution (in mM): 14.4 $NaHCO_3$, 5.9 KCl, 2. 5 $MgSO_4$, 120.9 NaCl, 1.2 NaH_2PO_4, 2.5 $CaCl_2$, 11.5 glucose (pH 7.4). Excised trigeminal and dorsal root ganglia were then cut into small pieces using fine forceps and incubated in Krebs solution supplemented with 1mg/ml collagenase (type 1A, Sigma) ~37° C for 40-50 min. The tissue was then allowed to cool to room temperature and used within 6 hours. For neonatal mice (P8-P9) similar procedures were employed with the exception that tissue incubation time in collagenase-containing solution was abbreviated to 20-30 minutes.

Tissue fragments were transferred to a recording chamber mounted on the stage of an upright microscope (E600 FN, Nikon, Tokyo, Japan) equipped with differential interference contrast

optics and epifluorescence, which was used to visualize EGFP-expressing SGCs. Whole-cell recordings were made at room temperature using a Multiclamp 700A amplifier (Axon Instruments, Union City, CA) with fire-polished borosilicate pipettes (3–7 MΩ, Sutter Instruments, Novato, CA). Intracellular solution consisted (in mM): 125 KGluconate, 2 $CaCl_2$, 2 $MgCl_2$, 10 EGTA, 10 HEPES, 0.5 NaGTP, and 2 Na_2ATP, pH with KOH (pH 7.2). Bath solution consisted of Krebs solution described above. All traces were sampled at 5–10 kHz and low-pass filtered at 2 kHz. The input resistance of the cell was calculated based on the steady state current change during application of a 10 mV hyperpolarizing pulse. The membrane capacitance of the SGCs was calculated from the transient capacitance currents during application of a 10 mV hyperpolarizing pulse. Capacitance compensation and series resistance compensation were not employed. Liquid junction potential (15 mV) was corrected offline using the liquid junction potential calculator in Clampex 10.1 (Axon Instruments).

Statistics

Numerical values are given as mean ± SE. All comparisons across conditions were made by using Student's t-test or analyses of variance (ANOVA) and Tukey's or Bonferroni's tests for multiple comparisons. Differences were considered statistically significant when $p < 0.05$.

Results

Kir4.1 channels are expressed in satellite glial cells in sensory ganglia

We used a BAC EGFP mouse line (Kir4.1-EGFP) to examine the cellular sites of Kir4.1 subunit expression in mouse peripheral sensory ganglia. In this mouse line, EGFP expression is driven by Kir4.1 promoter regulatory sequences and faithfully reports the cellular sites of Kir4.1 subunit expression. We have previously shown the correlation of expression between EGFP and Kir4.1 in several glial cell types in the central nervous system (Tang et al., 2009). When we examined the expression of EGFP in trigeminal ganglia we observed strong fluorescence signals in the cytoplasm of small, fusiform cells surrounding larger neuronal somata (Figure 1A-C). The fluorescence signals for EGFP remained in fixed tissue and upon co-immunostaining for glutamine synthetase (GS) we observed the overlap of EGFP and GS expression (Figure 1A-C). Based on the morphology of the EGFP+ cell bodies and the double labeling analysis we identified these cells as SGCs. Similar results were also obtained in dorsal root ganglia (Figure 1D-F). Immunostaining using a previously characterized anti-Kir4.1 antibody (Tang et al., 2009) shows considerable co-localization of Kir4.1 immunostaining and intrinsic EGFP signals (Supplementary Figure 1 A-F). Some immunostaining signals for Kir4.1 were also observed in the neuronal somata but these were taken as non-specific signals given that they remained in ganglia isolated from a Kir4.1 -/- mouse. NeuN+ cells, on the other hand, did not express EGFP in any samples analyzed (results not shown). These results indicate the specific expression of Kir4.1 in SGCs in mouse peripheral sensory ganglia.

Inward currents in SGCs have a pharmacological profile consistent with Kir4.1 channel expression

While the previous results demonstrate expression of Kir4.1 in SGCs, they do not reveal whether Kir4.1 contributes significantly to the K^+ conductance in these cells. We made use of electrophysiological and pharmacological techniques, as well as a Kir4.1 channel knockout mouse line to address this question. SGCs were visually identified using EGFP as a guide in acutely dissociated trigeminal or dorsal root ganglia preparations (Figure 2A). In wild-type adult mice (P30-P50), current clamp recordings showed that these cells never fired action potentials after injection of large depolarizing currents. They were also highly hyperpolarized (~-78 to -80 mV, Table 1) and input resistances of SGCs were very low and similar ($p>0.05$) in cells recorded from trigeminal ganglia (17.3 ± 0.8 MΩ, n= 20) or dorsal root ganglia (17.4 ± 1.8 MΩ, n= 8). These membrane properties are consistent with previous reports on trigeminal

and dorsal root ganglia SGCs (Gola et al., 1993, Konishi, 1996, Cherkas et al., 2004, Zhang et al., 2009). Voltage clamp recordings from trigeminal ganglia SGCs (Figure 2B) revealed large inward and outward currents in response to de- and hyperpolarizing 300 ms voltage steps from a holding potential of -70 mV. Inward and outward currents displayed little time dependent activation or inactivation. Plotting steady state current amplitudes as a function of the applied voltage revealed that the current-voltage (*I-V*) relationships displayed an almost linear profile from -160 to +30 mV (Figure 2C). Similar currents were observed in SGCs recorded from dorsal root ganglia (Supplemental Figure 2A).

In order to identify Kir currents, we determined the *I-V* relationships in the absence and presence of 100 μM extracellular barium, which blocks Kir channels by occlusion of the conduction pore (Doupnik et al., 1995). In recordings from adults SGCs from trigeminal ganglia, we observed an almost complete blockade of inward currents upon application of 100 μM barium with a less pronounced blockade of the outward currents (Figure 2B-D). The barium-sensitive current (Figure 2D) shows an inwardly rectifying profile with considerable outward current. As predicted for a K^+-selective current, the reversal potential of the barium-sensitive current (-74 mV) closely matched the estimated equilibrium potential for K^+ (E_K) (-78 mV). In addition to being blocked by barium, Kir channels are also blocked by external cesium in a voltage-dependent manner (Doupnik et al., 1995). Application of 1mM cesium resulted in a pronounced inhibition of trigeminal ganglia SGC currents at hyperpolarized membrane potentials that became less pronounced at more depolarized membrane potentials (Figure 3A). Taken together, the sensitivity of SGCs inward currents to extracellular barium and cesium suggests that these currents are mediated by Kir channels. Recently, it has been shown that the tricyclic anti-depressants such as desipramine reversibly inhibits Kir4.1 currents in a concentration-dependent manner (Su et al., 2007). These compounds are somewhat selective for Kir4.1 channels in comparison to other Kir channels such as Kir2.1 and Kir3.1/Kir3.2 channels. Bath application of 100 μM desipramine did indeed result in blockade of inward currents (82 ± 3 % at −140mV) albeit with time-dependent relief of blockade at hyperpolarized membrane potentials (Figure 3B). The average blockade of barium, cesium and desipramine measured at -140mV amounted to near 90% (Figure 3C).

Kir channel currents recorded from Kir4.1 +/- SGCs are reduced by about 50%

The lack of Kir subunit specific blockers has hampered the direct assessment of the Kir channel composition in various glial types including SGCs. We made use of a Kir4.1 knockout mouse line (Kir4.1 -/-) as an alternative method to assess the contribution of Kir4.1 in SGC membrane properties. We have shown previously that in this mouse line the expression of Kir4.1 channel is absent in various glial cell types including Müller cells, oligodendrocytes and astrocytes (Kofuji et al., 2000, Neusch et al., 2001, Tang et al., 2009). We first evaluated whether there were changes in the steady-state mRNA expression levels of Kir4.1 in the heterozygous Kir4.1 +/- mice. Mouse trigeminal ganglia cDNA was used for quantitative RT-PCR (see material and methods). As shown in Figure 4A, Kir4.1 mRNA levels in P30-P50 trigeminal ganglia of Kir4.1 +/- animals showed a ~ 35% reduction compared to wild-type while in P8-P9 the reduction was of ~ 54% (Figure 4B). This gene dosage effect led us to reason that if Kir4.1 is the principal Kir subunit expressed in SGCs we would observe a decrease of inward current density in the heterozygous mice by about 50 %. To test this, we compared the SGCs current densities at -140 mV in the trigeminal ganglia in P30-50 wild-type and Kir4.1 +/- mice (Figure 4C, D). In the heterozygous Kir4.1 +/- mice SGCs, the current density was indeed reduced by 46% in comparison to wild-type (-173.4 ± 16.3 pA/pF, n = 16 vs -323.2 ± 36.3 pA/pF, n = 20) and the input resistance increased by about twofold (30.2 ± 2.2 MΩ, n = 16 vs 17.3 ± 0.8 MΩ, n = 20) (Table 1). Similar reduction of expression of inward currents was also observed in SGCs recorded from dorsal root ganglia (Table 1). There were no significant changes in the cell capacitance or resting membrane potential of SGCs recorded from Kir4.1 +/- mice in

comparison to aged-matched wild-type littermates (Table 1). Thus, the reduction of inward current in the SGCs from heterozygous mice strongly supports the notion that Kir4.1 subunit is crucial in mediating the inward conductance in trigeminal and dorsal root ganglia SGCs.

Kir channel currents is largely absent in SGCs from Kir4.1-/- mice

A more direct way to assess the role of Kir4.1 subunit in SGCs is to record from homozygous Kir4.1-/- mice. These mice rarely survive beyond two weeks of age (Neusch et al., 2001) so we performed recordings in Kir4.1 -/- and aged matched wild-type and heterozygous Kir4.1 +/- littermates at P8 to P9 stages. At these stages (neonatal) the SGCs recorded from trigeminal ganglia already displayed the electrophysiological properties observed in adult animals, i.e. deeply hyperpolarized membrane potentials (-79 ± 1 mV in wild-type and -79 ± 1 mV in Kir4.1 +/- mice) and low input resistance (40.2 ± 2.3 MΩ in wild-type and 92.8 ± 8.8 MΩ in Kir4.1 +/- mice)(Table 1). Whole cell voltage clamp recordings of SGCs from wild-type and Kir4.1 +/- neonatal mice show barium-sensitive currents that accounted for almost all inward currents (Figure 5). Interestingly the inward currents exhibited a pronounced time dependent inactivation at membrane potentials more negative than -140 mV (Figure 5A), reminiscent of "variably rectifying" astrocytes in the neonatal hippocampus (Zhou et al., 2006). However quite distinct electrophysiological properties were seen in SGCs from age-matched Kir4.1 -/- mice (Table 1). First, they displayed significantly ($p < 0.05$) more depolarized resting membrane potentials (-65 ±1 mV, n=11) in comparison to wild-type (-79 ± 1 mV, n=17). Second, input resistance of SGCs recorded from Kir4.1 -/- mice were about 40 fold larger than wild-type (1647.5 ± 168.5 MΩ vs 40.2 ± 2.3 MΩ). Third, step depolarizations using voltage-clamp of SGCs in Kir4.1 -/- mice elicited substantial outward currents while inward currents at hyperpolarized membrane potentials were almost absent (Figure 6A-B). Furthermore, addition of 100 μM extracellular barium was largely ineffective in reducing either inward or outward currents (Figure 6C). Finally, there was a conspicuous insensitivity of inward currents to Kir channel blockers such as cesium and desipramine (Figure 6D). Overall the inward current densities from Kir4.1 -/- mice decreased by 98%, compared with age-matched wild-type mice (Figure 6E)(Table 1).

Kir4.1is likely to associate with Kir5.1 in SGCs

Although the previous results indicate that Kir4.1 underlies the inward currents in SGCs they do not address the question whether they function as homomeric or heteromeric assemblies. It has been suggested that Kir4.1 associates with Kir5.1 subuunits in kidney, retina and brain to form a channel with distinct functional properties (Tanemoto et al., 2000, Ishii et al., 2003, Lachheb et al., 2008). In heterologous expression systems, Kir4.1-Kir5.1 heteromeric channels but not Kir4.1 homomeric channels are susceptible to inhibition upon intracellular PKC activation (Rojas et al., 2007). We hypothesized that if Kir4.1 subunits associated with Kir5.1 subunits in trigeminal ganglia SGCs, then we should see a reduction in SGC current upon application of PMA, an activator of PKC. Recordings from adult SGCs from trigeminal ganglia SGCs show that PKC activation via application of PMA (0.1μmol), significantly inhibited inward currents (Figure 7A) while the inactive analogue of PMA (4α-PDD, 0.1μmol) failed to do so (Figure 7B). On average, at -140 mV, PMA decreased inward currents by 39 ± 4% (n=6) and 4α-PDD by 3 ± 3 % (n=6)($P < 0.05$)(Figure 7C). These results suggest that Kir4.1 associate with Kir5.1 subunits in trigeminal ganglia SGCs.

Discussion

Our results demonstrate that inward K^+ currents in SGCs from trigeminal and dorsal root ganglia have pharmacological and functional profiles consistent with being mediated almost exclusively by Kir4.1 channels. Glial cells in many areas of the central nervous system exhibit a large resting K^+ conductance that is attributed to expression of barium-sensitive Kir channels

(Kofuji and Connors, 2003). However, a functional assessment of Kir4.1 channel expression in SGCs in sensory ganglia had been lacking. Our results show, for the first time, that partial (Kir4.1 +/- mice) or complete (Kir4.1 -/- mice) genetic ablation of Kir4.1 yields corresponding decreases on the barium-sensitive inward currents of SGCs. The parallel change on Kir4.1 transcript levels and barium-sensitive inward currents in these mouse lines strongly argues that Kir4.1 accounts for almost all inward conductance in sensory SGCs. Our results also show that in SGCs Kir4.1 probably co-assembles with Kir5.1 to form heteromeric Kir4.1/Kir5.1 channels.

It is generally accepted that the foremost mechanism for K^+ buffering of the extracellular space in the brain is "spatial K^+ buffering". In this process, glial cells dissipate local K^+ gradients by transferring K^+ ions from areas of high to low $[K^+]_o$ (Kofuji and Newman, 2004). Similar to astrocytes in the central nervous system, spatial buffering currents in SGCs may dissipate $[K^+]_o$ increases by flowing through a syncytium of coupled glial cells with high membrane permeability to K^+ ions. SGCs are moderately coupled to each other (Huang et al., 2005) and our study indicates that these cells display high conductance of K^+ ions. The low input resistance on the order of 17 MΩ in mouse SGCs is equivalent to that found in hippocampal astrocytes (Seifert et al., 2009) and in retinal Muller cells (Kofuji et al., 2000) and reflects the high densities of Kir4.1 channels in the plasma membrane of all these glial cell types. Therefore the functional substrates for spatial K^+ buffering appear to be in place in sensory ganglia. Direct support of this hypothesis has been lacking but recent results employing siRNA in rats are intriguing. Transient decreases of either Kir4.1 channel or connexin 43 expression in trigeminal ganglia SGCs enhance spontaneous or evoked facial nociceptive responses mimicking a neuropathic pain-like behavior (Ohara et al., 2008, Vit et al., 2008). These findings suggest that alterations of K^+ conductive pathways into or between SGCs augment the excitability of primary sensory neurons as expected for an impaired spatial K^+ spatial buffering in sensory ganglia.

One overlooked assumption of "spatial K^+ spatial buffering" is that the glial cell membranes are selectively permeable to K^+ at rest and only poorly permeable to anions such as chloride otherwise the "spatial buffering" currents would be shunted (Kofuji and Newman, 2004). Chloride channels have been detected in SGCs surrounding sympathetic neurons in the rabbit coeliac ganglion (Gola et al., 1993) raising the possibility that other K^+ buffering mechanisms (e.g. passive KCl reuptake) are also relevant in sensory ganglia. To our knowledge the relative permeability for anions has not yet been determined in either trigeminal or dorsal root ganglia. In either case, the Kir4.1 channels are expected to provide the bulk of K^+ entry pathways given their high density in SGCs plasma membrane.

Another proposed role of Kir4.1 in macroglia is in setting their resting membrane potentials, which are usually more hyperpolarized than their neuronal counterparts (Butt and Kalsi, 2006). We now report that SGCs from Kir4.1 knockout mouse, the resting membrane potentials are significantly more depolarized (-65 mV in Kir4.1 -/- vs -79 mV in Kir4.1 +/+). Depolarization of glial cells could conceivably affect a number of voltage-dependent processes including the clearance of extracellular glutamate by the electrogenic glutamate transporter GLAST. However, neuronal somatic release of glutamate in sensory ganglia has yet to be established and at the moment it is unclear whether glutamate transporters in SGCs perform an analogous role to astrocytes in the central nervous system.

It is interesting to notice that SGCs recorded from wild type mice trigeminal or dorsal root ganglia exhibited almost identical electrophysiological properties in regard to resting membrane potential, input resistance and current density at -140 mV (Table 1). The Kir4.1 channels may exert similar role in both types of sensory ganglia because SGCs from these two sites show: 1) similar levels of EGFP expression in the reporter mouse Kir4.1 EGFP, 2)

comparable inward current densities at hyperpolarized membrane potentials, 3) similar decreases of inward currents in the Kir4.1 +/- mice. These findings somewhat contradict a previous report that indicated the lack of Kir4.1 immunoreactivity in rat dorsal root ganglia (Hibino et al., 1999) which could be accounted by either species differences or antibody specificity.

While our results clearly indicate the dominant role of Kir4.1 subunits in forming the Kir conductance in SGCs they do not discard the possibility that Kir4.1 function as heteromeric assemblies (Butt and Kalsi, 2006). Immunoprecipitation studies from many tissues have suggested that Kir4.1 may hetero-oligomerize with Kir5.1 subunits (Hibino et al., 2004). Kir5.1 is a subunit which does not produce a functional channel as homomultimer (Pessia et al., 1996) but when co-assembled with Kir4.1 it forms channels more susceptible to PKC-mediated inhibition in heterologous expression systems (Rojas et al., 2007). We found that the Kir conductance in SGCs are indeed partially inhibited by modulators of PKC lending some support that the native channels in SGCs function as heteromeric Kir4.1/Kir5.1 assemblies. Moreover outwardly rectifying currents remained in SGCs from Kir4.1 -/- mice and the membrane potential of these cells still remained relatively polarized suggesting the presence of other K^+ conductances in these glial cells. Possible candidates are the two-pore domain K^+ channels such as TWIK-1 and TREK-1 which underlie part of the passive conductance of mature hippocampal astrocytes (Seifert et al., 2009, Zhou et al., 2009). TREK-1, in particular is an attractive candidate given its relative insensitivity to extracellular barium (Zhou et al., 2009) and voltage-dependent gating, which leads to strong outward rectification (Maingret et al., 2002).

Recently, missense or nonsense mutations in the Kir4.1 encoding gene (KCNJ10) have been linked with human syndromes characterized by epilepsy, ataxia, deafness and renal tubolapathy (Bockenhauer et al., 2009, Scholl et al., 2009). Because our results indicate the central role of Kir4.1 in sensory ganglia it will be interesting to assess whether affected individuals also harbor abnormal mechanical, thermal or nociceptive thresholds. Development of Kir4.1 channel specific openers may be potential targets for the treatment of disorders characterized by neuronal hyperexcitability or inherited diseases linked to Kir4.1 hypofunction.

Supplementary Material

Refer to Web version on PubMed Central for supplementary material.

Acknowledgments

This project was funded by Grant EY12949 from the National Institutes of Health. We thank Darwin Hang for excellent technical support.

References

Bockenhauer D, Feather S, Stanescu HC, Bandulik S, Zdebik AA, Reichold M, Tobin J, Lieberer E, Sterner C, Landoure G, Arora R, Sirimanna T, Thompson D, Cross JH, van't Hoff W, Al Masri O, Tullus K, Yeung S, Anikster Y, Klootwijk E, Hubank M, Dillon MJ, Heitzmann D, Arcos-Burgos M, Knepper MA, Dobbie A, Gahl WA, Warth R, Sheridan E, Kleta R. Epilepsy, ataxia, sensorineural deafness, tubulopathy, and KCNJ10 mutations. The New England journal of medicine 2009;360:1960–1970. [PubMed: 19420365]

Butt AM, Kalsi A. Inwardly rectifying potassium channels (Kir) in central nervous system glia: a special role for Kir4.1 in glial functions. J Cell Mol Med 2006;10:33–44. [PubMed: 16563220]

Cherkas PS, Huang TY, Pannicke T, Tal M, Reichenbach A, Hanani M. The effects of axotomy on neurons and satellite glial cells in mouse trigeminal ganglion. Pain 2004;110:290–298. [PubMed: 15275779]

Doupnik CA, Davidson N, Lester HA. The inward rectifier potassium channel family. Curr Opin Neurobiol 1995;5:268–277. [PubMed: 7580148]

Dublin P, Hanani M. Satellite glial cells in sensory ganglia: their possible contribution to inflammatory pain. Brain Behav Immun 2007;21:592–598. [PubMed: 17222529]

Gola M, Niel JP, Delmas P, Jacquet G. Satellite glial cells in situ within mammalian prevertebral ganglia express K+ channels active at rest potential. The Journal of membrane biology 1993;136:75–84. [PubMed: 8271274]

Hanani M. Satellite glial cells in sensory ganglia: from form to function. Brain Res Brain Res Rev 2005;48:457–476. [PubMed: 15914252]

Hibino H, Fujita A, Iwai K, Yamada M, Kurachi Y. Differential assembly of inwardly rectifying K+ channel subunits, Kir4.1 and Kir5.1, in brain astrocytes. The Journal of biological chemistry 2004;279:44065–44073. [PubMed: 15310750]

Hibino H, Horio Y, Fujita A, Inanobe A, Doi K, Gotow T, Uchiyama Y, Kubo T, Kurachi Y. Expression of an inwardly rectifying K(+) channel, Kir4.1, in satellite cells of rat cochlear ganglia. The American journal of physiology 1999;277:C638–644. [PubMed: 10516093]

Huang TY, Cherkas PS, Rosenthal DW, Hanani M. Dye coupling among satellite glial cells in mammalian dorsal root ganglia. Brain research 2005;1036:42–49. [PubMed: 15725400]

Ishii M, Fujita A, Iwai K, Kusaka S, Higashi K, Inanobe A, Hibino H, Kurachi Y. Differential expression and distribution of Kir5.1 and Kir4.1 inwardly rectifying K+ channels in retina. American journal of physiology 2003;285:C260–267. [PubMed: 12686518]

Isomoto S, Kondo C, Kurachi Y. Inwardly rectifying potassium channels: their molecular heterogeneity and function. The Japanese journal of physiology 1997;47:11–39. [PubMed: 9159640]

Kofuji P, Ceelen P, Zahs KR, Surbeck LW, Lester HA, Newman EA. Genetic inactivation of an inwardly rectifying potassium channel (Kir4.1 subunit) in mice: phenotypic impact in retina. J Neurosci 2000;20:5733–5740. [PubMed: 10908613]

Kofuji P, Connors NC. Molecular substrates of potassium spatial buffering in glial cells. Mol Neurobiol 2003;28:195–208. [PubMed: 14576456]

Kofuji P, Newman EA. Potassium buffering in the central nervous system. Neuroscience 2004;129:1045–1056. [PubMed: 15561419]

Konishi T. Developmental and activity-dependent changes in K+ currents in satellite glial cells in mouse superior cervical ganglion. Brain research 1996;708:7–15. [PubMed: 8720853]

Kubo Y, Adelman JP, Clapham DE, Jan LY, Karschin A, Kurachi Y, Lazdunski M, Nichols CG, Seino S, Vandenberg CA. International Union of Pharmacology. LIV. Nomenclature and molecular relationships of inwardly rectifying potassium channels. Pharmacological reviews 2005;57:509–526. [PubMed: 16382105]

Lachheb S, Cluzeaud F, Bens M, Genete M, Hibino H, Lourdel S, Kurachi Y, Vandewalle A, Teulon J, Paulais M. Kir4.1/Kir5.1 channel forms the major K+ channel in the basolateral membrane of mouse renal collecting duct principal cells. Am J Physiol Renal Physiol 2008;294:F1398–1407. [PubMed: 18367659]

Maingret F, Honore E, Lazdunski M, Patel AJ. Molecular basis of the voltage-dependent gating of TREK-1, a mechano-sensitive K(+) channel. Biochemical and biophysical research communications 2002;292:339–346. [PubMed: 11906167]

Neusch C, Rozengurt N, Jacobs RE, Lester HA, Kofuji P. Kir4.1 potassium channel subunit is crucial for oligodendrocyte development and in vivo myelination. J Neurosci 2001;21:5429–5438. [PubMed: 11466414]

Nichols CG, Lopatin AN. Inward rectifier potassium channels. Annu Rev Physiol 1997;59:171–191. [PubMed: 9074760]

Ohara PT, Vit JP, Bhargava A, Jasmin L. Evidence for a role of connexin 43 in trigeminal pain using RNA interference in vivo. Journal of neurophysiology 2008;100:3064–3073. [PubMed: 18715894]

Ohara PT, Vit JP, Bhargava A, Romero M, Sundberg C, Charles AC, Jasmin L. Gliopathic pain: when satellite glial cells go bad. Neuroscientist 2009;15:450–463. [PubMed: 19826169]

Olsen ML, Sontheimer H. Functional implications for Kir4.1 channels in glial biology: from K+ buffering to cell differentiation. J Neurochem 2008;107:589–601. [PubMed: 18691387]

Pessia M, Tucker SJ, Lee K, Bond CT, Adelman JP. Subunit positional effects revealed by novel heteromeric inwardly rectifying K+ channels. The EMBO journal 1996;15:2980–2987. [PubMed: 8670799]

Pfaffl MW. A new mathematical model for relative quantification in real-time RT-PCR. Nucleic acids research 2001;29:e45. [PubMed: 11328886]

Rojas A, Cui N, Su J, Yang L, Muhumuza JP, Jiang C. Protein kinase C dependent inhibition of the heteromeric Kir4.1-Kir5.1 channel. Biochimica et biophysica acta 2007;1768:2030–2042. [PubMed: 17585871]

Scholl UI, Choi M, Liu T, Ramaekers VT, Hausler MG, Grimmer J, Tobe SW, Farhi A, Nelson-Williams C, Lifton RP. Seizures, sensorineural deafness, ataxia, mental retardation, and electrolyte imbalance (SeSAME syndrome) caused by mutations in KCNJ10. Proceedings of the National Academy of Sciences of the United States of America 2009;106:5842–5847. [PubMed: 19289823]

Seifert G, Huttmann K, Binder DK, Hartmann C, Wyczynski A, Neusch C, Steinhauser C. Analysis of astroglial K+ channel expression in the developing hippocampus reveals a predominant role of the Kir4.1 subunit. J Neurosci 2009;29:7474–7488. [PubMed: 19515915]

Su S, Ohno Y, Lossin C, Hibino H, Inanobe A, Kurachi Y. Inhibition of astroglial inwardly rectifying Kir4.1 channels by a tricyclic antidepressant, nortriptyline. The Journal of pharmacology and experimental therapeutics 2007;320:573–580. [PubMed: 17071817]

Tanemoto M, Kittaka N, Inanobe A, Kurachi Y. In vivo formation of a proton-sensitive K+ channel by heteromeric subunit assembly of Kir5.1 with Kir4.1. The Journal of physiology 2000;525(Pt 3):587–592. [PubMed: 10856114]

Tang X, Taniguchi K, Kofuji P. Heterogeneity of Kir4.1 channel expression in glia revealed by mouse transgenesis. Glia 2009;57:1706–1715. [PubMed: 19382212]

Vit JP, Ohara PT, Bhargava A, Kelley K, Jasmin L. Silencing the Kir4.1 potassium channel subunit in satellite glial cells of the rat trigeminal ganglion results in pain-like behavior in the absence of nerve injury. J Neurosci 2008;28:4161–4171. [PubMed: 18417695]

Zhang H, Mei X, Zhang P, Ma C, White FA, Donnelly DF, Lamotte RH. Altered functional properties of satellite glial cells in compressed spinal ganglia. Glia 2009;57:1588–1599. [PubMed: 19330845]

Zhou M, Schools GP, Kimelberg HK. Development of GLAST(+) astrocytes and NG2(+) glia in rat hippocampus CA1: mature astrocytes are electrophysiologically passive. Journal of neurophysiology 2006;95:134–143. [PubMed: 16093329]

Zhou M, Xu G, Xie M, Zhang X, Schools GP, Ma L, Kimelberg HK, Chen H. TWIK-1 and TREK-1 are potassium channels contributing significantly to astrocyte passive conductance in rat hippocampal slices. J Neurosci 2009;29:8551–8564. [PubMed: 19571146]

Abbreviations

CNS	Central Nervous System
EGFP	Enhanced Green Fluorescent Protein
EGTA	Ethylene Glycol Tetraacetic Acid
GLAST	Glutamate-Aspartate Transporter
GS	Glutamine Synthetase
HEPES	4-(2-hydroxyethyl)-1-piperazineethanesulfonic acid
I-V	current-voltage
Kir	Inwardly Rectifying Potassium
PBS	Phosphate Buffered Solution
PCR	Polymerase Chain Reaction
SGC	Satellite Glial Cell

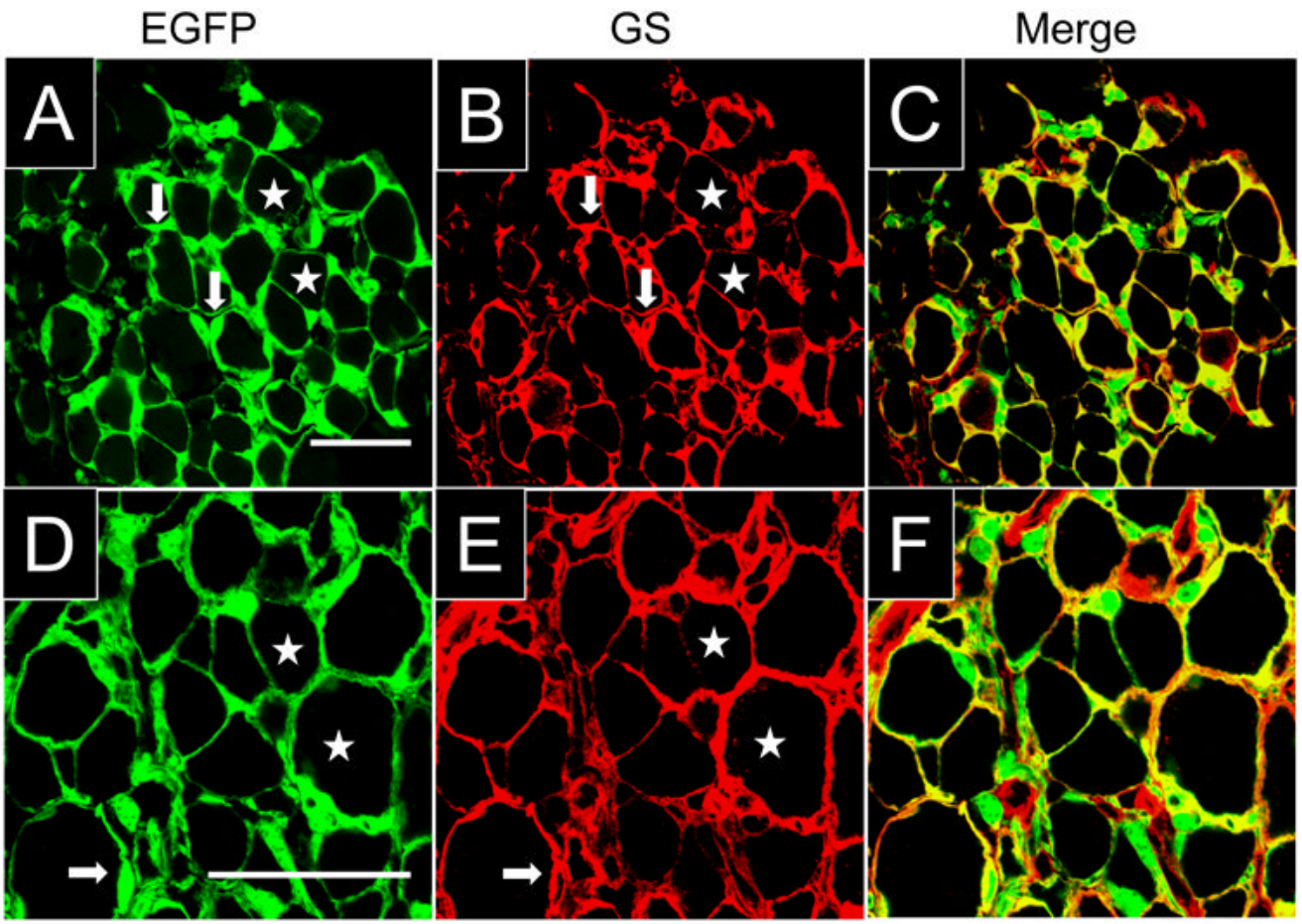

Figure 1. EGFP is colocalizes with glutamine synthetase (GS) in trigeminal and dorsal root ganglia SGCs

(A-C) Immunostaining for GS and intrinsic fluorescence of EGFP in Kir4.1-EGFP trigeminal ganglion. EGFP and GS co-localized in small fusiform cells (arrows) surrounding larger neurons (stars). The expression of GS and cell morphology indicate that EGFP+ cells constitute SGCs. **(D-F)** Immunostaining for GS and intrinsic fluorescence of EGFP in the Kir4.1-EGFP dorsal root ganglion. There is again co-localization of Kir4.1 and EGFP signals in SGCs (arrows) enveloping larger neurons (stars). Scale bars: 50 μm.

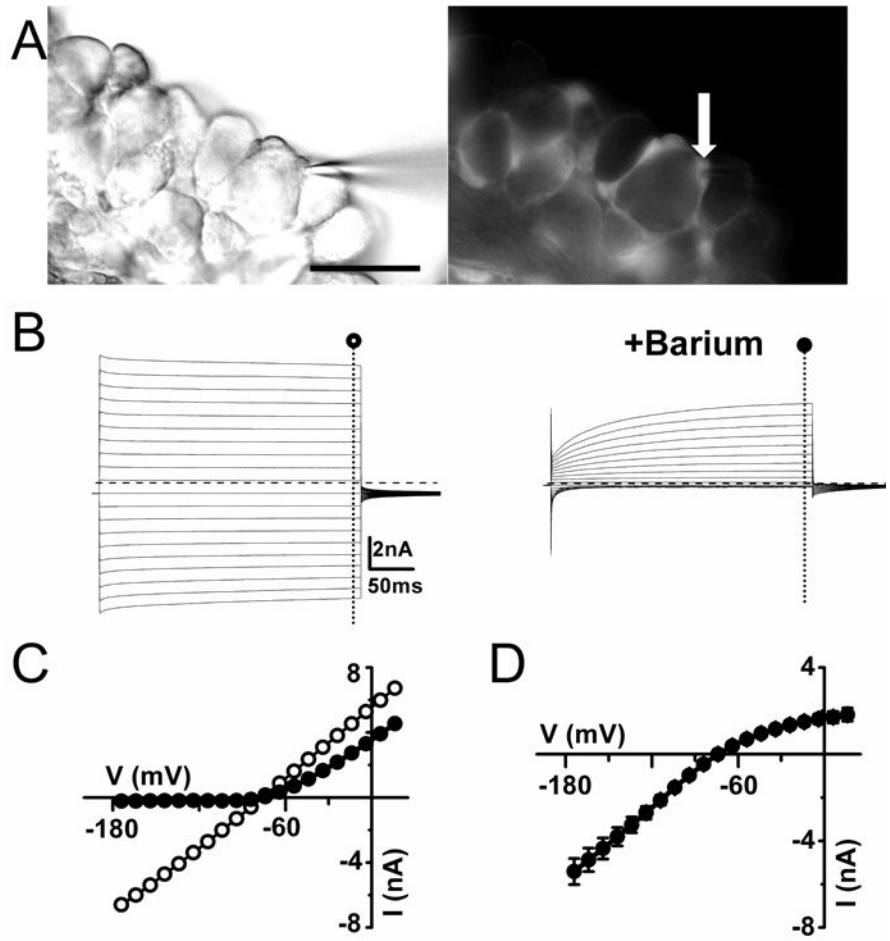

Figure 2. SGCs from wild-type trigeminal ganglion express a barium-sensitive inward conductance

(A) Electrophysiological recordings were performed on SGCs in partially intact ganglia from Kir4.1-EGFP mice. DIC image in the left panel shows the recording pipette on the fluorescent cell shown in the right panel (arrow). Right panel shows epifluorescence image of fluorescent SGCs. **(B)** Inward and outward currents were evoked by voltage steps from -160 to +30 mV for 300 ms in the in the absence (○) and presence (●) of 100μM barium in the bath. Dashed lines indicate zero current level. **(C)** Current magnitudes at the end of the voltage step are plotted against membrane potential for a representative cell the absence (○) and presence (●) of 100μM barium in the bath. **(D)** Average barium-sensitive currents plotted against membrane potential show an inward rectification profile (n=9). Scale bar: (A) 50μm.

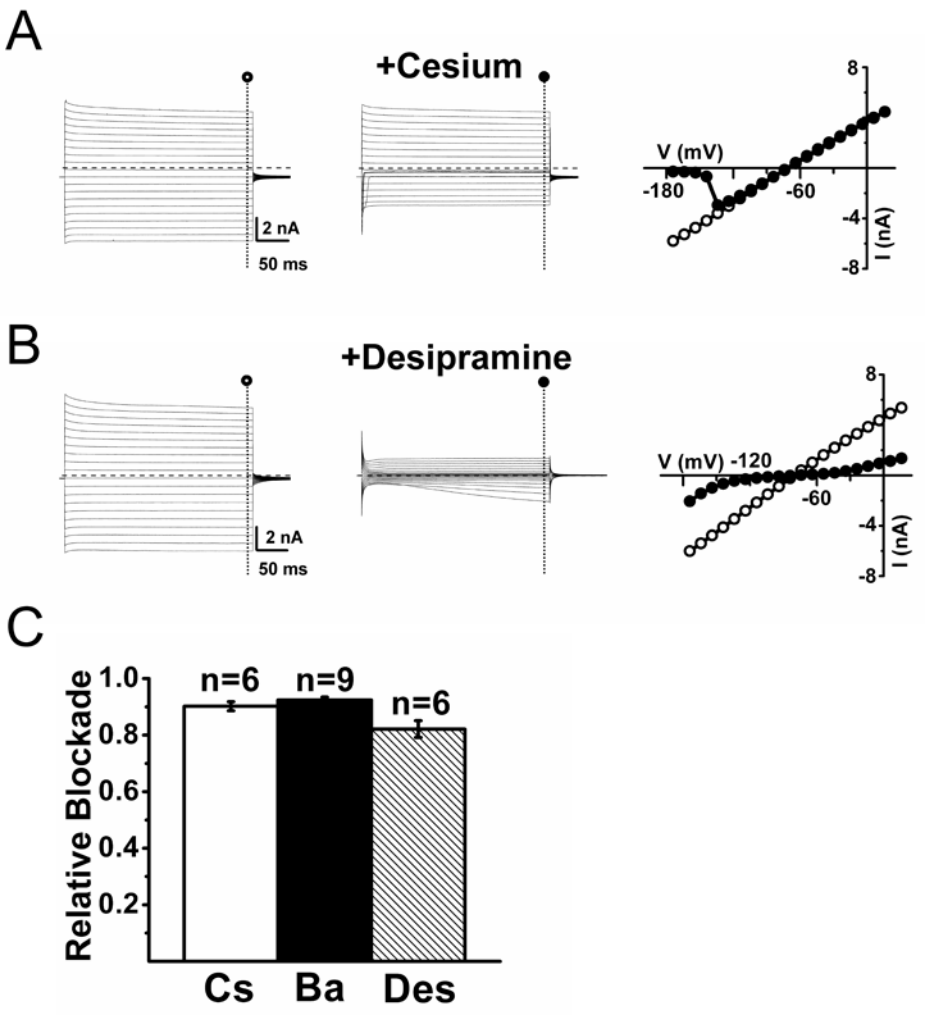

Figure 3. SGCs from wild-type trigeminal ganglion express cesium-sensitive and desipramine-sensitive inward conductances

(A) Inward and outward currents evoked upon voltage steps from -160 to +30 mV in the absence (○, left panel) and presence (●, middle panel) of 1 mM extracellular cesium. Right panel shows the current-voltage relationship for a representative cell in the absence (○) and presence (●) of 1 mM extracellular cesium, demonstrating the strong blockade of inward currents at membrane potentials more hyperpolarized than -130mV. Dashed lines represent zero current level. **(B)** Inward and outward currents evoked upon voltage steps from -160 to +30 mV in the absence (○, left panel) and presence (●, middle panel) of 100 μM desipramine in the bath. Right panel shows the current-voltage relationship for a representative cell in the absence (○) and presence (●) of 100 μM desipramine in the bath. Current-voltage relationships for evoked currents show some relief of blockade at membrane potentials more hyperpolarized than -140 mV. Dashed lines represent zero current level. **(C)** Summary of the relative blockade at -140 mV for cesium (Cs), barium (Ba) or desipramine (Des) shows a relative blockade between 80 to 90% of the inward currents at -140 mV.

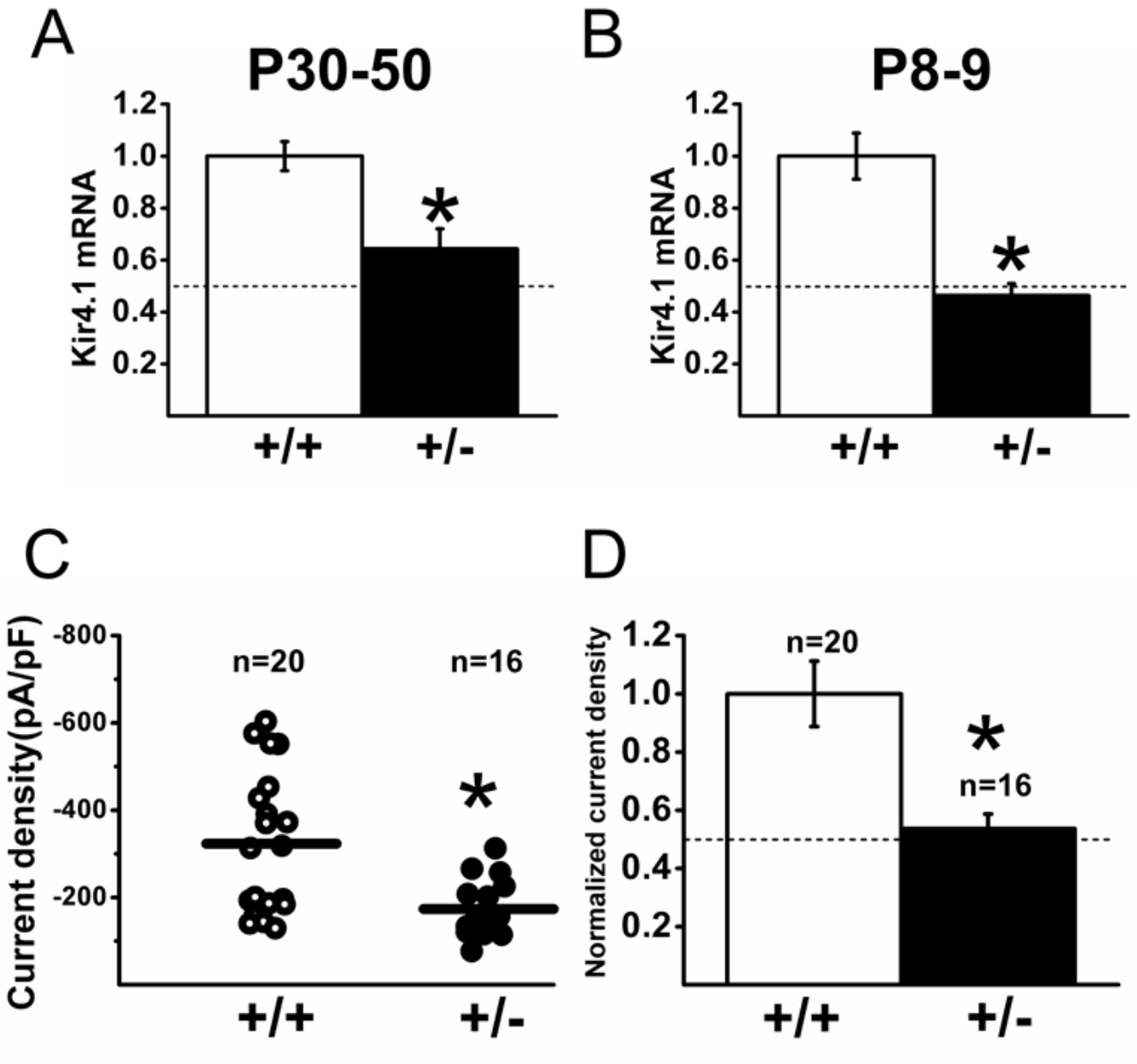

Figure 4. Kir4.1 transcript levels and inward currents are diminished in SGCs from trigeminal ganglia from Kir4+/- mice

(A-B) Kir4.1 transcript levels were analyzed in trigeminal ganglia from Kir4.1 +/- and wild-type littermates using real time RT-PCR. Summary of Kir4.1 mRNA expression in P30-P50 (left panel) and P8-P9 (right panel) shows the significant reduction of transcript levels in the Kir4.1 +/- mice ($P<0.05$). Dashed lines represent 50% of wild-type transcript levels. **(C)** Summary of the current density for SGCs from adult wild-type (circle) and heterozygous Kir4.1 +/- (dot) trigeminal ganglions (measured at -140 mV). Significantly smaller currents were recorded from SGCs in Kir4.1 +/- mice compared to wild-type ($P<0.05$). **(D)** Currents in the SGCs of Kir4.1 +/- mice were normalized against the currents obtained in wild-type littermates. Normalized current density for SGCs from (C) shows a significant reduction of 46% in current density recorded from heterozygous (dot) mice compared to wild-type ($P<0.05$). Dashed line indicates the half of the normalized mean value of wild-type current density.

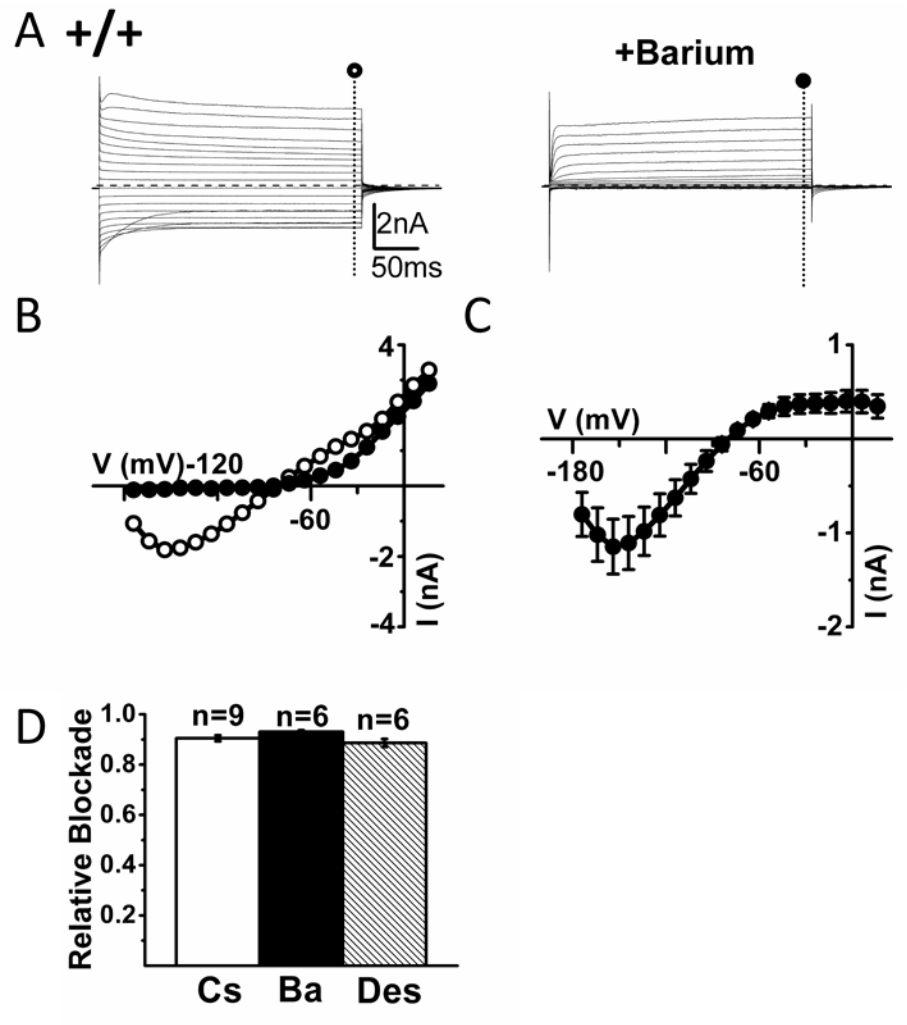

Figure 5. Neonatal (P8-P9) wild-type mouse trigeminal ganglia SGCs express large inward currents sensitive to extracellular barium

(A) Left panel shows inward and outward currents evoked upon voltage steps of -160 to +30 mV in a representative trigeminal ganglion SGC from a wild-type neonatal (P8-P9) mouse. In the right panel the cell was exposed to 100 μM extracellular barium with blockade of inward current with little effect on outward currents. Dashed lines indicate zero current level. **(B)** *I-V* relationships in the absence (○) and presence (●) of 100μM barium in the bath for a representative cell from the SGC shown in (A). **(C)** Mean *I-V* relationships of barium-sensitive currents (n=6) in neonatal wild-type mouse trigeminal ganglia SGCs. **(D)** Summary of the relative blockade at -140 mV for cesium (Cs), barium (Ba) or desipramine (Des).

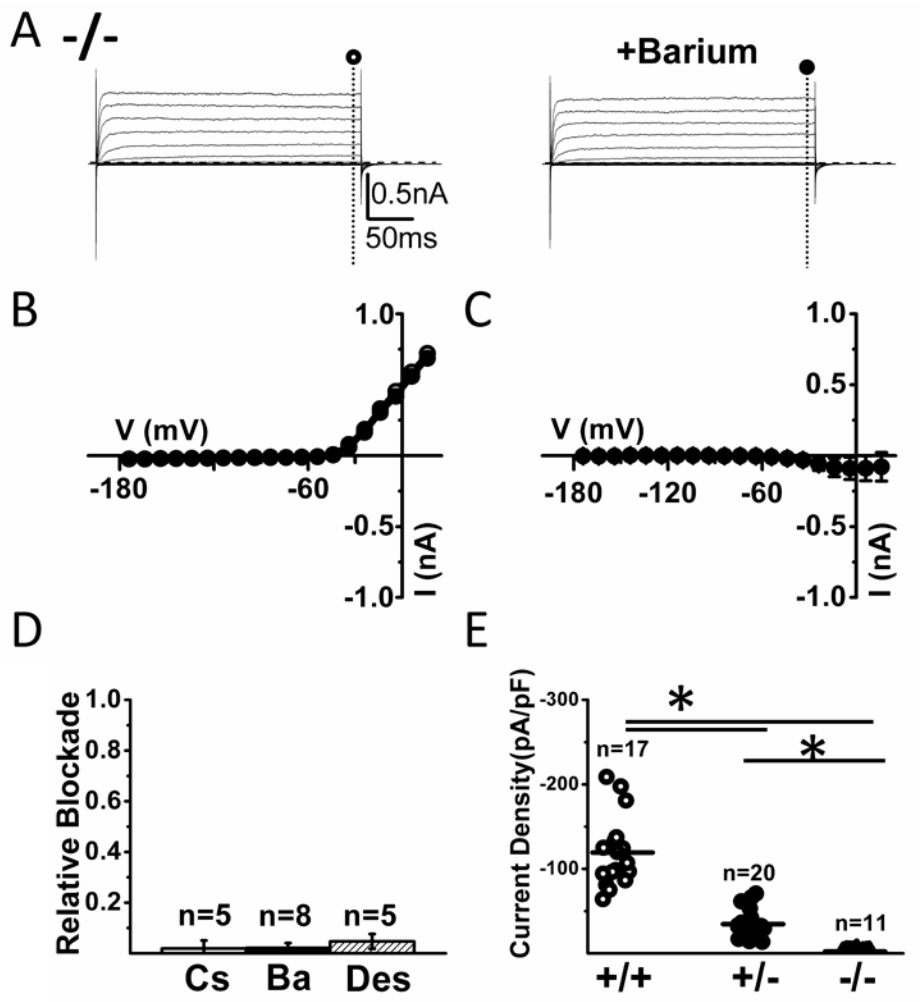

Figure 6. Lack of inward currents and barium-sensitive currents in the neonatal (P8-P9) Kir4.1 -/- mice SGCs

(A) Left panel shows inward and outward currents evoked upon voltage steps of -160 to +30 mV in a representative trigeminal ganglion SGC from Kir4.1 -/- mouse. Notice the almost complete absence of inward currents. In the right panel the cell was exposed to 100 μM extracellular barium with no apparent effect. Dashed lines indicate zero current level. **(B)** *I-V* relationships from the cell recorded in (A). **(C)** Mean *I-V* relationships of barium-sensitive currents recorded from Kir4.1 -/- mouse SGCs (n=9). **(D)** Summary of the relative blockade of currents at -140 mV for cesium (Cs), barium (Ba) or desipramine (Des) from Kir4.1 -/- mice shows the lack of expression of Kir channels. **(E)** Current density for SGCs from neonatal wild-type (circle), Kir4.1 +/- (dot) and Kir4.1 -/- (triangle) trigeminal ganglions (measured at -140 mV, 300ms) shows a graded reduction of inward currents with decreased expression of Kir4.1.

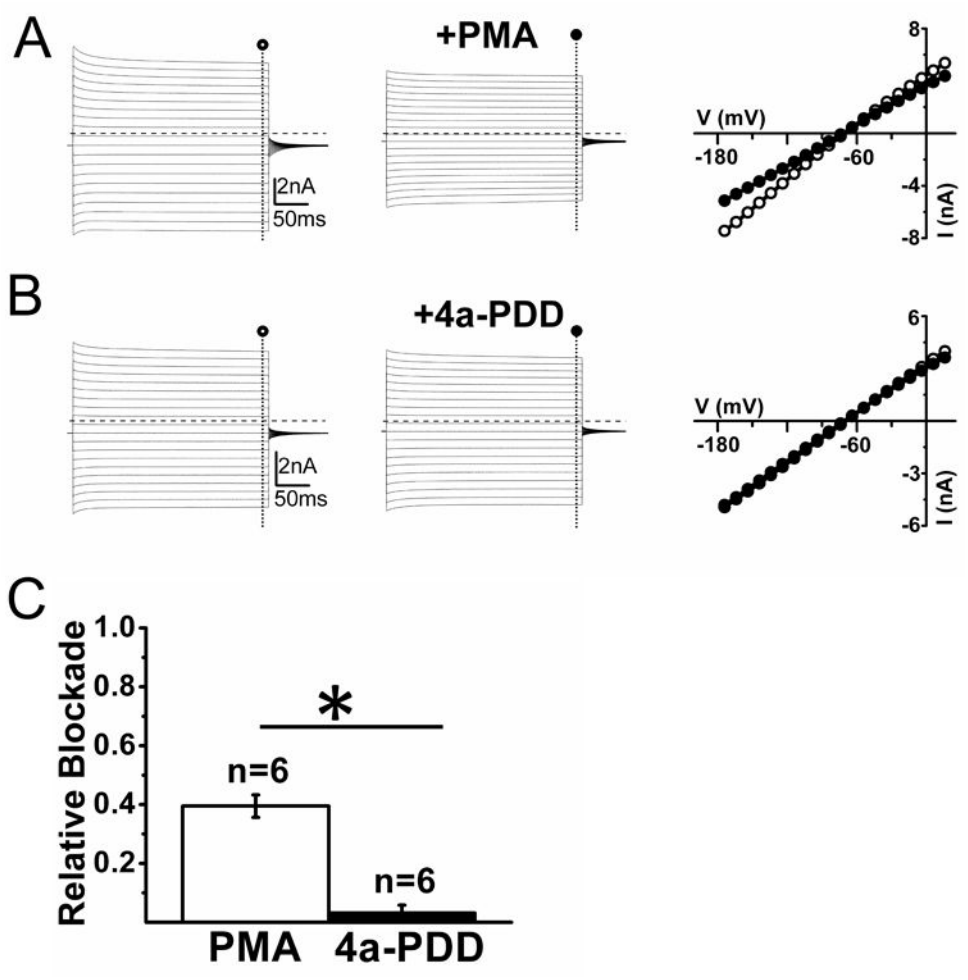

Figure 7. Evidence for functional Kir4.1-Kir5.1 heteromultimers in of adult (P30-P50) wild-type trigeminal ganglion SGCs

(A) Current traces from a representative cell before (left panel) and after (middle panel) application of 0.1 μM of the PKC activator PMA show the partial inhibition of inward currents upon PMA application. Right panel shows *I-V* relationship for the same cell in the absence (○) and presence (●) of 0.1μmM of the PKC activator PMA. Dashed lines represent zero current level. **(B)** Current traces from a representative cell before (left panel) and after (middle panel) application of the inactive analog of PMA 4α-PDD at 0.1μmM, which failed to exhibit any changes. Right panel shows *I-V* relationship for the same cell in the absence (○) and presence (●) of 4α-PDD at 0.1μmM. The inactive analog of PMA 4α-PDD at 0.1μmM failed to elicit any changes in either inward or outward currents Dashed lines represent zero current level. **(C)** Summary of the relative blockade of currents at -140 mV for PMA and 4a-PDD shows significant inhibition for PMA ($P<0.05$).

Table 1

Cell capacitance, resting membrane potential, input resistance, current density of SGCs in trigeminal (TG) and dorsal root ganglia (DRG)

Resting membrane potential (RMP). The asterisk (*) represents significant values (P< 0.05), when compared to the data obtained in Kir4.1 wild-type group.

TG / **Age**	**Cell capacitance (pF)**	**RMP (mV)**	**Input resistance (MΩ)**	**Current density (pA/pF @ - 140mV)**
Kir4.1 +/+ (P30-P60) (n=20)	17.7 ± 2.0	-78 ± 1	17.3 ± 0.8	-323.2 ± 36.3
Kir4.1 +/- (P30-P60) (n=16)	15.4 ± 1.3	-78 ± 1	30.2 ± 2.2*	-173.4 ± 16.3*
Kir4.1 +/+ (P7-P10) (n=17)	15.1± 1.3	-79 ± 1	40.2 ± 2.3	-119.3 ± 10.2
Kir4.1 +/- (P7-P10) (n=20)	17.8 ± 1.2	-79 ± 1	92.8 ± 8.8*	-34.6 ± 3.7*
Kir4.1 -/- (P7-P10) (n=11)	21.0 ± 2.6*	-65 ± 1*	1647.5 ± 168.5*	-2.2 ± 0.3*
DRG / Age	Cell capacitance (pF)	RMP (mV)	Input resistance (MΩ)	Current density (pA/pF @ - 140mV)
Kir4.1 +/+ (P30-P60) (n=8)	16.8± 1.9	-80 ± 1	17.4 ± 1.8	-302.9 ± 30.4
Kir4.1 +/- (P30-P60) (n=10)	17.4 ± 2.3	-79 ± 1	35.7 ± 4.4*	-146.7 ± 18.0*